

Maser Emission toward the Infrared Dark Cloud G359.94+0.17 Seen in Silhouette against the Galactic Center

Shuji DEGUCHI,

*Nobeyama Radio Observatory, National Astronomical Observatory,
and Department of Astronomical Science, The Graduate University for Advanced Studies,
Minamimaki, Minamisaku, Nagano 384-1305*

Daniel TAFOYA,

*Department of Physics and Astronomy, Graduate School of Science and Engineering,
Kagoshima University, 1-21-35 Korimoto, Kagoshima 890-0065*

and

Nagisa SHINO

*Graduate School of Science and Engineering, Yamaguchi University,
1677-1 Yoshida, Yamaguchi, Yamaguchi 753-8512*

(Received 2011 April 26; accepted 2011 October 11)

Abstract

The infrared dark cloud G359.94+0.17 is a conspicuous, opaque cloud, which is seen in silhouette against the Galactic center. We found unexpectedly strong (~ 50 Jy) maser emission of CH₃OH at 44 GHz with additional weak 22 GHz H₂O maser and 43 GHz SiO thermal emissions toward this cloud. Detections of these molecular lines indicate that strong star forming activities are proceeding in this cloud, which were not reported previously despite of numerous works toward the Galactic center. The line profiles of the NH₃ inversion lines at 23 GHz indicate that G359.94+0.17 is composed of mainly two clouds with $V_{\text{lsr}} = 0$, and 15 km s^{-1} overlapped on the line of sight. The maser emission is associated with the 15 km s^{-1} cloud, suggesting that it is located at the Norma spiral arm.

Key words: masers — ISM: clouds — ISM: dust, extinction — ISM: molecules

1. Introduction

One of the infrared dark clouds seen in projection to the Galactic center, G359.94+0.17 (Dutra & Bica 2002), is the most distinctive dark cloud seen within 0.3° of the Galactic center. (In Figure 1, we show a part of the Spitzer/GLIMPSE false-color image¹ in this direction for an illustration purpose; Stolovy et al. 2006.) In the area of a size of a few arc minutes toward this cloud, almost no star in the Galactic bulge is seen. This cloud causes substantial undersampling of AGB stars in the Galactic bulge in this direction (for example, see figure 1 of Deguchi et al. 2004).

Though numerous studies of molecular clouds toward the Galactic center have been made in the past (for example, see Morris & Serabyn 1996; Yusef-Zadeh et al. 2009), a very limited amount of works were made to investigate this interesting cloud G359.94+0.17, or more in general, the dark clouds toward the Galactic center. This is possibly because these clouds are supposed to be in the foreground and not directly associated with the Galactic center. However, without cautious studies, it is hasty to decide the distances to these clouds.

Nagayama et al. (2009) carefully studied the extinction due to dust grains in the K_S band within the $5^\circ \times 2^\circ$ area in this direction. They found that the $V_{\text{lsr}} = 15 - 20 \text{ km s}^{-1}$ CO emission is associated with these clouds. Based on the star counts in the JHK bands, they estimated the distances to these clouds to be $3.2 - 4.2 \text{ kpc}$, and suggested that these clouds are located in the Norma spiral arm. The dark clouds that they studied have extinction of $A_K = 0.6 - 1.0$. Though their contour map (figure 2 of Nagayama et al. 2009) indicated that the $V_{\text{lsr}} = 15 - 20 \text{ km s}^{-1}$ CO emission is also associated with the dark cloud G359.94+0.17, they excluded this cloud from their study, possibly because K -band extinction of this dark cloud is too high for their star-count study.

In this paper, we report the detection of maser emission of CH₃OH and H₂O toward the dark cloud, G359.94+0.17. The presence of the maser emission toward this dark cloud suggests that strong star forming activities are proceeding in this infrared opaque cloud. We have also observed thermal emission of SiO and NH₃. Based on these observations, we discuss the nature of this interesting dark cloud which is seen in projection to the Galactic center.

2. Observations and Results

Observations of the dark cloud G359.94+0.17 were made on 2011 February 26 with the Nobeyama 45-m tele-

¹ available at http://apod.nasa.gov/apod/fap/image/0906/mwcenter_spitzer_big.jpg; The thick dark patch is also clearly seen in the 2MASS and MSX false-color images as well as on WISE (NASA's Wide-field Infrared Survey Explorer mission) images at various infrared wavelengths.

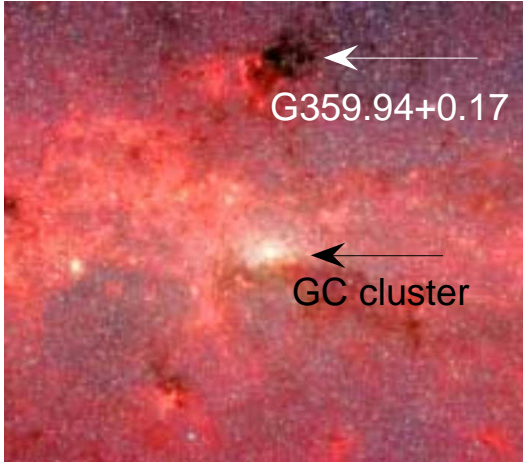


Fig. 1. A part of the Spitzer false-color image (3.6–8 μm) of the Galactic center region ($0.55^\circ \times 0.5^\circ$; left is the direction of increasing the Galactic longitude). White arrow indicates the dark cloud G359.94+0.17 and black arrow indicate the Galactic center star cluster surrounding Sgr A* at $(l, b) = (359.944^\circ, -0.046^\circ)$.

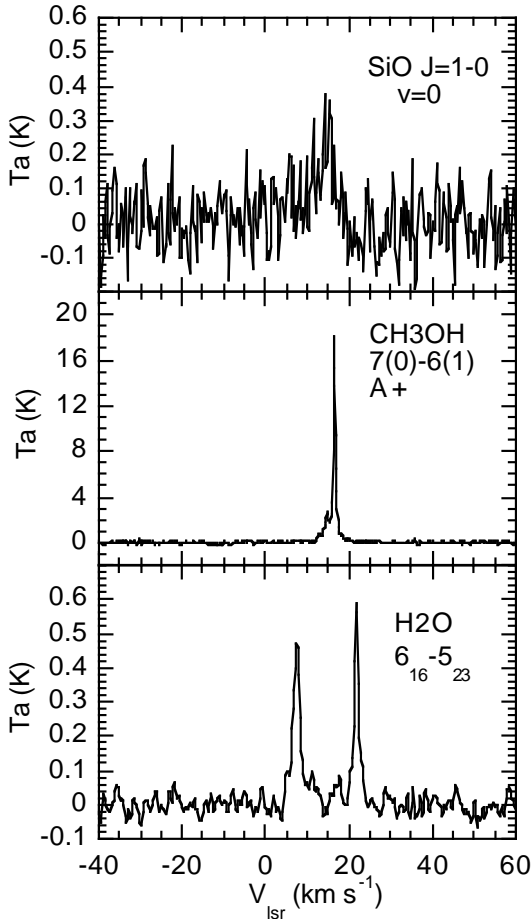


Fig. 2. Spectra of the SiO $J = 1-0, v = 0$ (top), CH₃OH 7(0)–6(1) A+ (middle), and H₂O $6_{16}-5_{23}$ (bottom) transitions toward the dark cloud G359.94+0.17 (H₂O; 17h44m53.20s, $-28^\circ 54' 04.8''$).

scope in the H₂O and NH₃ lines between 22 and 24 GHz, and on March 10 in the SiO and CH₃OH lines between 42 and 44 GHz. The half-power full beam width (HPFBW) was about 70'' at 22 GHz and 40'' at 43 GHz. We used cooled HEMT receivers, H22 and H40 ($T_{\text{sys}} \sim 100$ –250 K) and acousto-optical spectrometer arrays with high (40 kHz; AOS-H) and low (250 kHz; AOS-W) resolutions having 2048 channels each. The conversion factor of the antenna temperature ($\equiv T_a^*$) to the flux density was ~ 2.9 Jy K^{−1} at 43 GHz and it is 2.8 Jy K^{−1} at 22 GHz. The accuracy of pointing of the telescope was about 5''. The observational results for the CH₃OH, SiO, and H₂O lines are summarized in table 1 and their spectra are shown in Figure 2.

The H₂O maser emission consists of two components at $V_{\text{lsr}} = 7.6$ and 21.6 km s^{−1}. To check the positions of H₂O maser emission, we have made the 5-point 40''-grid cross mapping observation as follows. From the 2MASS *K*-band image, we found with eye inspection that the position of the darkest part of the cloud is (R.A., Decl.)=(17h44m54.0s, $-28^\circ 54' 00''$) in epoch of *J*2000. After detecting H₂O masers at this position, we have performed the 5-point 40''-grid cross mapping of H₂O maser emission. From the integrated intensities of the H₂O maser components at each position of the grid, we computed the center positions of each water maser component, assuming that they are point sources. The resulted positions are (R.A., Decl.)=(17h44m53.65s, $-28^\circ 54' 04.1''$) for the $V_{\text{lsr}} = 7.6$ km s^{−1} component, and (R.A., Decl.)=(17h44m53.20s, $-28^\circ 54' 04.8''$) for the $V_{\text{lsr}} = 21.6$ km s^{−1} component in epoch of *J*2000, which corresponds to $(l, b) = (359.947^\circ, +0.154^\circ)$, and $(l, b) = (359.946^\circ, +0.155^\circ)$, respectively. It is known that the accuracy of pointing for the 45m telescope is about 5'' in the absolute position. Therefore, we assume that the water maser position given above is accurate at this level. These positions are approximately 1' east of the position of the dark cloud G359.94+0.17 given by Dutra & Bica (2002).

The mapping observations were also made for the NH₃ inversion lines simultaneously with the mapping for the H₂O maser line. The variations of the NH₃ 1(1) and 3(3) line profiles at 40'' separated positions are shown in Figure 3. Due to the hyperfine splitting, the NH₃ 1(1) line is separated into 5 groups with velocity separations of approximately $-19, -8, 8, 19$ km s^{−1} relative to the strongest central components (Rydbeck et al. 1977). Left panel of Figure 3 shows that the NH₃ 1(1) line profile is composed of 7 peaks, which suggests that the cloud has several different velocity components. The strongest peak of the NH₃ lines falls at $V_{\text{lsr}} \sim 15.2$ km s^{−1} at position (00'', 00'') [= (17h44m54.0s, $-28^\circ 54' 00''$)] and the second strongest peak at $V_{\text{lsr}} \sim 0.3$ km s^{−1} which exhibits stronger emission at position (−40'', 0''). In addition we found a weak enhancement of emission at $V_{\text{lsr}} \sim 80$ km s^{−1} at position (+40'', 0''), which is indicated by arrows in figure 3. This emission exhibits a broad line width of more than 30 km s^{−1}.

Table 1. Observed line intensities of the CH₃OH, SiO, and H₂O lines.

Frequency (GHz)	Molecule	Transition	T_a (peak) (K)	V_{lsr} (peak) (km s ⁻¹)	Integ. Ints. (K km s ⁻¹)	r.m.s (K)
44.06949	CH ₃ OH	7(0)–6(1) A+	18.029	16.5	19.245	0.087
43.423858	SiO	1–0 $v=0$	0.409	15.3	1.648	0.087
22.235077	H ₂ O	6(1,6)–5(2,3)	0.485	7.6	1.459	0.024
22.235077	H ₂ O	6(1,6)–5(2,3)	0.606	21.6	1.295	0.024

3. Discussions

A large number of infrared dark clouds have been cataloged in the first and forth quadrants of the Galactic plane using the 8.3 μ m MSX images (Simon et al. 2006a) and the Spitzer GLIMPSE and MIPS data (Peretto & Fuller 2009). Their nature has been well studied through molecular lines (Simon et al. 2006b). The IR dark clouds contain compact cores with a mass range 10 – 2100 M_\odot (Rathborne et al. 2006), and smaller fragments with masses down to $\sim 0.1 M_\odot$ (Peretto & Fuller 2010). Approximately one third of these cores show evidence of active star formation (Jackson et al. 2008b). About 12% of these infrared dark clouds exhibit H₂O maser emission (Wang et al. 2006). It seems that the dark cloud G359.94+0.17 shares similar properties in several respects as the known IR dark clouds except for its massive feature. It is listed as the dark cloud core G359.91+00.17a [$(l, b)=(359.938, +0.174)$] in the catalog of Simon et al. (2006a), where "a" indicates the multiplicity index code in the dark cloud complex G359.91+00.17.

3.1. Thermal emission of NH₃ and SiO

The intensity ratio between the NH₃ inversion lines can be used as a thermometer of the cloud (Danby et al. 1988). We calculated the rotational temperature of the observed clouds from the 1(1) and 2(2) line intensity ratio and summarized the result in table 2. We derived the rotational temperature from the 1(1) versus 2(2) line intensity ratio at each position and gave the result in table 2. They are in a range between 19 and 25 K. The intensity of the NH₃ sub-component at $V_{lsr} \sim 80$ km s⁻¹ is stronger at 40'' east of the mapping center. The absence of the hyperfine feature of this component in the 1(1) profile indicates that this cloud has large internal motion, which flattens out the hyperfine feature. In contrast, the hyperfine feature of the components appearing at $V_{lsr} \sim -10 - +30$ km s⁻¹ is clearly seen in right panel of Figure 3, which indicates that internal motions of these clouds are less than a few km s⁻¹. It exhibits a complex variation in the hyperfine feature at different positions. We identified that the major components are two clouds with $V_{lsr} = -0.3$ and 15.3 km s⁻¹, which are easily seen in the 3(3) spectra, because the influence of the hyperfine splittings is marginal in the 3(3) spectra at this noise level.² We named them as primary

and secondary components. In addition, we call the 80 km s⁻¹ component as tertiary. The intensity of these three components varies depending on the positions. Because the grid separation 40'' is just slightly larger than the half-power half-beam width (HPHBW $\sim 35''$) of the telescope, and because the hyperfine lines from the different components of the cloud are blended in the line profile, it is cumbersome to clearly separate all the velocity components from the observed profile in this observation. We computed a contribution of each component by successive decomposition of the original line profile into the standard NH₃ profiles with hyperfine splitting, and gave these numbers in the foot of table 2. The profiles shown in Figure 3 are well fitted by introducing two major components with $V_{lsr} = 0.3$ and 15.2 km s⁻¹ (with additional very minor contributions ($< 10\%$) from the -3.5 and -24.5 km s⁻¹ components.)

We also computed the column density of the NH₃ at the 1(1) levels [see details in Liszt et al. (2006)] and listed it in the last column in table 2. The column density gives the optical extinction $A_v = 35$ and 28 at the position $(-40'', 0'')$ and $(0'', 0'')$, respectively, and $A_v = 13$ for tertiary component at the position $(+40'', 0'')$. Here we have assumed that the NH₃ abundance is 2×10^{-9} per H₂ (Liszt et al. 2006), and that the level populations of ammonia are thermalized at the observed rotational temperature, and the relation between hydrogen column density and optical extinction as $N_H = 2.2 \times 10^{21} \text{ cm}^{-2} A_v$ (Güver & Özel 2009). Though it involves an uncertainty factor of 3 in the NH₃ abundance for these components of the cloud, the calculated extinction $A_v \sim 30$ ($A_K \sim 2$) is roughly consistent with the extinction estimated in this direction (Schultheis et al. 1998). The mass of the cloud can be estimated from the formula $M = 372 M_\odot \times (A_v/30) \times (D/4 \text{ kpc})^2 \times (\theta/1')^2$, which assumes a uniform cloud with a spherical shape (i.e., a depth being the same as a diameter of the cloud) using the above conversion ratio of A_v to N_H , where D and θ are the distance and angular diameter of the cloud [cf., eq. (10) of Marshall et al. (2009)] and $1' = 1.16$ pc at 4 kpc. Approximately these clouds contain a mass of 100–500 M_\odot in an area with an angular size of 1'.

We also detected the SiO $J=1-0$ $v=0$ thermal line at 43.4 GHz. SiO thermal emission is an indicator of an outflow in a star forming region (Downes et al. 1982). Thermal SiO emission ($J=1-0$ $v=0$) toward the Galactic center has been mapped using the Yebes 14m telescope (Martin-Pintado et al. 2000), but no emission was seen in

² Because the hyperfine intensities of the satellite components in the 3(3) line are negligibly small ($\sim 10\%$ in total; Coudert & Roueff 2006), the line can be regarded as a single component

at the noise level in the present paper.

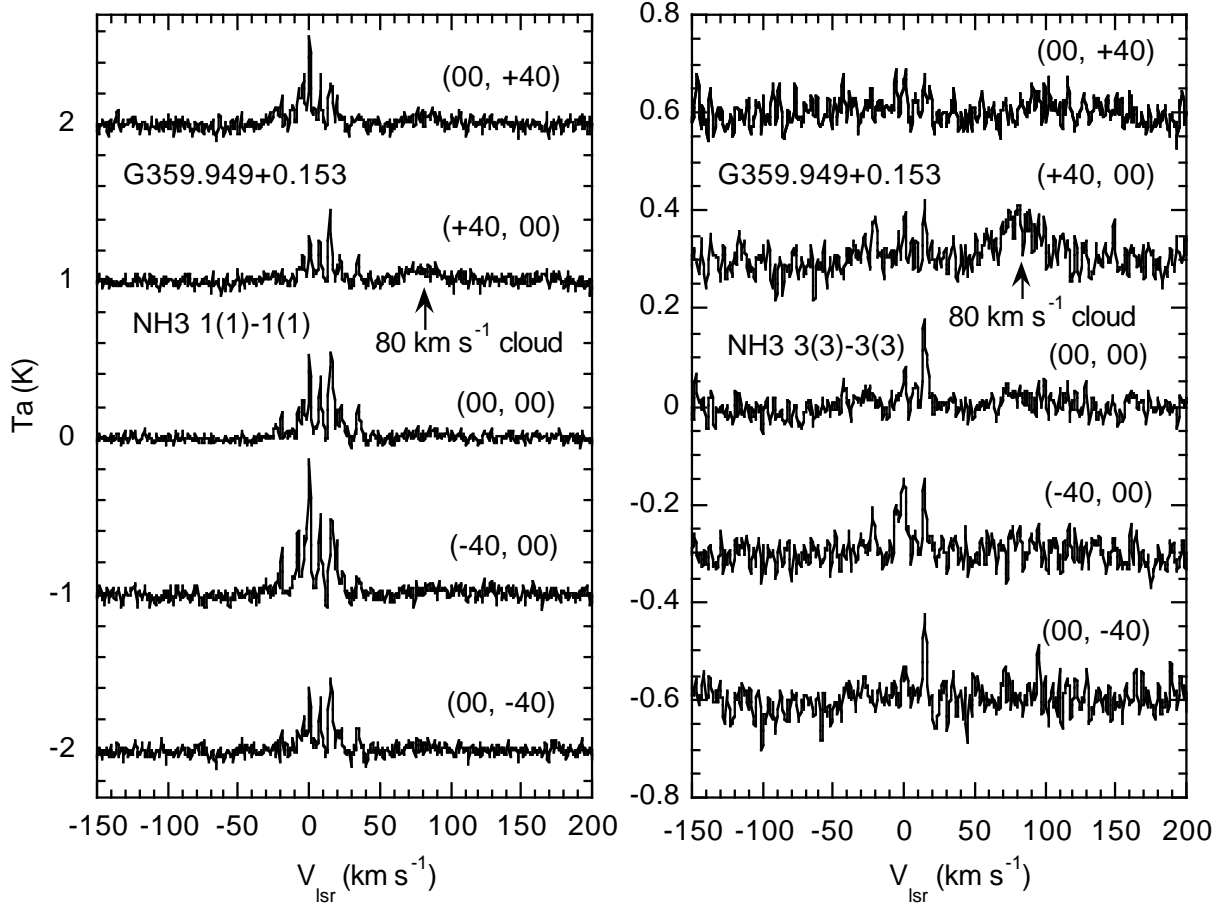


Fig. 3. 5-point 40''-grid cross mapping spectra of the NH₃ 1(1) (left) and 3(3) (right) lines. The center velocity of the 1(1) line refers to 23.69451 GHz. The mapping center (0,0) is the position of (R.A.=17h44m54.0s, Decl.= -28°54'00''; J2000), and the position shifts are made in the R.A. and Decl. directions. In order to reduce noises, three-channel running mean is applied for the NH₃ 3(3) spectra. The emission around $V_{\text{lsr}} = 80 \text{ km s}^{-1}$, which is indicated by the arrow, is detected at +40'' east more clearly in the 3(3) line. The influence of the hypersplittings is marginal in the 3(3) spectra at this noise level.

Table 2. Observed line intensity of the NH₃ inversion lines and rotational temperature.

component	position [#] (", ")	I.I. 1(1) (K km s ⁻¹)	I.I. 2(2) (K km s ⁻¹)	I.I. 3(3) (K km s ⁻¹)	T_R ([1/2]) (K)	$N_c[\text{NH}_3(1,1)]$ 10^{13} cm^{-2}
primary (+secondary) [†]	(-40,0)	9.147	3.429	1.832	24.4	1.7
secondary (+primary) [‡]	(0,0)	7.082	2.259	2.233	22.8	1.4
tertiary ($V_{\text{lsr}} = 80 \text{ km s}^{-1}$)	(+40,0)	2.792	0.647	2.767	19.4	0.7

[#] (R.A., Decl.) position shift from (17h44m54.0s, -28°54'00'') in J2000.

[†] approximately 28% of emission comes from the secondary (15.2 km s⁻¹) component.

[‡] approximately 47% of emission comes from the primary (-3.5 - 0.3 km s⁻¹) component.



Fig. 4. Spitzer false-color image of the G359.94+0.17 region ($7' \times 4'$; left is the direction of increasing the Galactic longitude). Cross, circle, and square indicate the positions of the H_2O and CH_3OH masers ($V_{\text{lsr}} = 7 - 21 \text{ km s}^{-1}$) found in this paper, the 6 GHz CH_3OH maser found by Chambers et al. (2011) ($V_{\text{lsr}} = -0.8 \text{ km s}^{-1}$), and the H_2O maser found by Taylor et al. (1993) ($V_{\text{lsr}} = -8.4 \text{ km s}^{-1}$).

their map at the position of the dark cloud G359.94+0.17.

3.2. H_2O and CH_3OH maser emission

Methanol masers are well known tracers of early stage of star formation. They are often classified into two categories – Class I and Class II (Menten 1991). The former shows maser action mainly in the 36 and 44 GHz lines, and the latter in the 6.7 and 12 GHz lines. Though this dichotomy for methanol maser sources is widely used, real objects occasionally exhibit confusing characteristics in high and low-mass star forming regions (Ellingsen 2005; Fontani et al. 2010).

Our detection of strong ($\sim 50 \text{ Jy}$) 44 GHz CH_3OH emission from the $V_{\text{lsr}} = 15 \text{ km s}^{-1}$ component cloud of G359.94+0.17 suggests that this cloud is categorized to a Class I source. Caswell (1996) made an unbiased survey for 6.7 GHz CH_3OH emission over a 2-square-degree area toward the Galactic center and found 23 maser sites. However, no emission was found toward G359.94+0.17. More recently, Chambers et al. (2011) detected weak 6.7 GHz CH_3OH maser emission at $V_{\text{lsr}} = -0.8 \text{ km s}^{-1}$ toward their “g22” cloud (G359.939+0.170) with the EVLA. The position of this 6.7 GHz CH_3OH maser was $1.5'$ west of our H_2O maser position and the radial velocity indicates that it is associated with the primary ($V_{\text{lsr}} \sim 0.3 \text{ km s}^{-1}$) component of the cloud. Taylor et al. (1993) made an unbiased survey of the H_2O maser sources in the inner $4^\circ \times 4^\circ$ area of the Galactic center with the VLA. They detected water maser emission with $V_{\text{lsr}} = -8.4 \text{ km s}^{-1}$ at the position (l, b)=(359.977, 0.168), which is $1.8'$ away from our H_2O maser position. Positions of these masers are shown in Figure 4. These previously found maser sources are not related with our 44 GHz CH_3OH cloud (the secondary component).

Class I line surveys in the past showed that giant molecular clouds exhibits strong 44 GHz emission with a peak intensity of typically $\sim 100 \text{ Jy}$ (e.g., see Haschick et al. 1990; Pratap et al. 2008). However, the surveys toward dark clouds, specially for EGOs (Extended Green Objects:

Cyganowski et al. 2009; Chambers et al. 2011) and for low-mass objects (Bae et al. 2011), showed that the 44 GHz CH_3OH emission is weak ($\sim 1 - 10 \text{ Jy}$) in general. Our detection of the strong ($\sim 50 \text{ Jy}$) 44 GHz CH_3OH maser emission in the dark cloud G359.94+0.17, together with the detections of H_2O and SiO emissions, suggests that a strong outflow activity comparable with those in massive molecular clouds is proceeding in this dark cloud.

3.3. Other molecular lines and distances

Jackson et al. (2008a) detected CS $J = 2-1$ line emission toward (l, b)=(359.94, +0.17) (assigned as MSXDC G359.91+00.17a) at $V_{\text{lsr}} = -0.9$ and 15.2 km s^{-1} (their table 1), which agree well with the radial velocities of our NH_3 primary and secondary components of G359.94+0.17. Carey et al. (1998) studied the IR dark cloud G359.94+0.17 in the H_2CO lines at 134 – 219 GHz, detecting the H_2^{12}CO and H_2^{13}CO at $V_{\text{lsr}} = -0.2 \text{ km s}^{-1}$. It is likely that this emission comes from the same cloud emitting the -0.9 km s^{-1} component of CS.

We found that the infrared dark cloud G359.94+0.17 is composed of three components with radial velocities, 0, 15 and 80 km s^{-1} . They may be associated with different foreground spiral arms, or with the Galactic center. Nagayama et al. (2009) estimated the distance of the 15–20 km s^{-1} dark clouds toward the Galactic center as 4 kpc from their star-count curve and the velocity gradient along the Galactic longitude. In addition, 6 dark clouds observed in 6 GHz and 44 GHz CH_3OH masers toward the Galactic center exhibit radial velocities in the range of $10 - 25 \text{ km s}^{-1}$ (Chambers et al. 2011). These facts indicate that they are in the same foreground spiral arm. Because the radial velocity of the secondary component of G359.94+0.17 is close to the above group of dark clouds, we infer that the secondary component has a similar distance as that of this group, i.e. $\sim 4 \text{ kpc}$. We also infer from the large line width ($\sim 30 \text{ km s}^{-1}$) and a high radial velocity ($\sim 80 \text{ km s}^{-1}$) of the tertiary component that the tertiary component is a cloud close to the Galactic center (e.g., see Oka et al. 2010). Because the tertiary component is seen only near the edge of the dark cloud G359.94+0.17, and because it is located near the Galactic center, this component is not a main source of opacity of G359.94+0.17. This 80 km s^{-1} cloud is clearly revealed in the map of the Galactic center region in the velocity range, $70 \text{ km s}^{-1} < V_{\text{lsr}} < 120 \text{ km s}^{-1}$, in the CS $J = 1-0$ line (Tsuboi et al. 1999), where our observed position ($l = 359.954^\circ$ and $b = 0.144^\circ$) is just at the edge of this cloud in the CS map.

The distance to the primary component ($V_{\text{lsr}} \sim 0 \text{ km s}^{-1}$) is difficult to guess. A very few 6 GHz CH_3OH masers exhibit nearly zero radial velocity toward the Galactic center: G359.138+0.031, G0.496+0.188, and G0.836+0.184 (Caswel et al. 2010), and G359.199+0.041 (g31; Chambers et al. 2011). All of them are located at positive Galactic latitude. The velocity gradient of $\sim 5 \text{ km s}^{-1}$ per degree may be derived from these sources. The large velocity gradient (Sofue 2006) indicates that they are likely associated with the Scutum-Crux arm at a

distance of ~ 2 kpc away from the Sun (at $l = 0^\circ$).

4. Conclusion

We have detected maser emission of CH_3OH and H_2O from the infrared dark cloud G359.94+0.17, which is seen in silhouette against the Galactic center on the near-infrared images. Because no star forming activity was reported in this cloud previously, it was thought that this was a tranquil cloud at low temperature. Our observations showed that three clouds at different distances are overlapped on the line of sight, and that this overlap of the clouds makes a very deep dark feature in silhouette against the Galactic center. Detections of CH_3OH and H_2O masers indicate that active star formation is proceeding in one of these clouds. SiO thermal emission also suggests a presence of mass outflow from young stars. The radial velocity of this cloud ($V_{\text{lsr}} \sim 15 \text{ km s}^{-1}$) is similar to the velocities of a chain of dark clouds which are seen at negative latitudes in the Galactic coordinates. It suggests that this cloud is likely located in the Norma spiral arm. It is inferred that the other component at $V_{\text{lsr}} \sim 0 \text{ km s}^{-1}$ is slightly closer, possibly associated with the Scutum-Crux arm. Though the present observation is limited only toward the direction of one distinctive dark cloud G359.47+0.17, it implies that diffuse clouds in the same spiral arm are widely spread in a larger ($\sim 1^\circ$) region toward the Galactic center. The foreground clouds must seriously contaminate large-scale molecular line maps in a limited velocity range, especially in the ^{12}CO and ^{13}CO maps toward the Galactic center (e.g., see Oka et al. 1998; Sofue 2006). Furthermore, Molinari et al. (2011) found a 100 pc twisted dust ring around the Galactic center on the dust temperature map created from 70 and 250 μm dust emissions. Because emission from the foreground dark clouds must also contaminate this map, each foreground IR dust clump must carefully be removed from the map. Studies of the infrared dark clouds with optically thin lines such as NH_3 would be very useful for separating the foreground spiral arms from the Galactic center clouds.

The authors thank Dr. Tomoharu Oka, Keio University, for useful comments.

References

Bae, J.-H., Kim, K.-T., Youn, S.-Y., Kim, W.-J., Byun, D.-Y., Kang, H., & Oh, C. S. 2011, arXiv1108.3878
 Carey, S. J., Clark, F. O., Egan, M. P., Price, S. D., Shipman, R. F., & Kuchar, T. A. 1998, *ApJ*, 508, 721
 Caswell, J. L., Fuller, G. A., Green, J. A., Avison, A., Breen, S. L. et al. 2010, *MNRAS*, 404, 1029
 Caswell, J. L. 1996, *MNRAS*, 283, 606
 Chambers, Edward T., Yusef-Zadeh, F., & Roberts, D. 2011, *ApJ*, 733, 42
 Chen, X., Ellingsen, S. P., Shen, Z.-Q., Titmarsh, A., & Gan, C.-G. 2011, *ApJS*, 196, 9
 Coudert, L. H. & Roueff, E. 2006, *A&A*, 449, 855 [and Erratum: *A&A*, 499, 347 (2009)]

Cyganowski, C. J., Brogan, C. L., Hunter, T. R., & Churchwell, E. 2009, *ApJ*, 702, 1615
 Danby, G., Flower, D. R., Valiron, P., Schilke, P., & Walmsley, C. M. 1988, *MNRAS*, 235, 229
 Deguchi, S., Imai, H., Fujii, T., Glass, I. S., Ita, Y., et al. 2004, *PASJ*, 56, 261
 Downes, D., Genzel, R., Hjalmarson, A., Nyman, L. A., & Ronnang, B. 1982, *ApJL*, 252, L29
 Dutra, C. M. & Bica, E. 2002, *A&A*, 383, 631
 Ellingsen, S. P. 2006, *MNRAS*, 359, 1498
 Fontani, F., Cesaroni, R., & Furuya, R. S. 2010, *A&A*, 517, 56
 Güver, T. & Özel, F. 2009, *MNRAS*, 400, 2050
 Haschick, A. D., Menten, K. M., & Baan, W. A. 1990, *ApJ*, 354, 556
 Jackson, J. M., Finn, S. C., Rathborne, J. M., Chambers, E., T. & Simon, R. 2008, *ApJ*, 680, 349
 Jackson, J. M., Chambers, E., T., Rathborne, J. M., Simon, R. & Zhang, Q. 2008, *ASPC*, 387, 44
 Liszt, H. S., Lucas, R., & Pety, J. 2006, *A&A*, 448, 253
 Marshall, D. J., Joncas, G., & Jones, A. P. 2009, *ApJ*, 706, 727
 Martin-Pintado, J., de Vicente, P., Rodríguez-Fernández, N. J., Fuente, A. & Planesas, P. 2000, *A&A*, 356, L5
 Menten, K. M. 1991, in *Atoms, ions and molecules: New results in spectral line astrophysics*, ed. A. Haschick, & P. T. P. Ho (San Francisco: ASP), *ASPC*, 16, 119
 Molinari, S., Bally, J., Noriega-Crespo, A., Compiègne, M., Bernard, J. P. et al. 2011, *ApJ*, 735, L33
 Morris, M., & Serabyn, E. 1996, *ARA&A*, 34, 645
 Nagayama, T., Sato, S., Nishiyama, S., Murai, Y., Nagata, T., et al. 2009a, *PASJ*, 61, 283
 Oka, T., Hasegawa, T., Sato, F., Tsuboi, M., & Miyazaki, A. 1998, *ApJS*, 118, 455
 Oka, T., Tanaka, K., Matsumura, S., Nagai, M., Kamegai, K., & Hasegawa, T. 2010, in "Proceedings of the Galactic Center Workshop" at Shanghai (arXiv1002.1526)
 Pratap, P., Shute, P. A., Keane, C., Battersby, C., & Sterling, S. 2008, *AJ*, 135, 1718
 Peretto, N., & Fuller, G.A. 2009, *A&A*, 505, 405
 Peretto, N., & Fuller, G.A. 2010, *ApJ*, 723, 555
 Rathborne, J. M., Jackson, J. M., & Simon, R. 2006, *ApJ*, 641, 389
 Rydbeck, O. E. H., Sume, A., Hjalmarson, A., Ellder, J., Ronnang, B. O., & Kollberg, E. 1977, *ApJ*, 215, L35
 Schultheis, M., Ganesh, S., Simon, G., Omont, A., Alard, C., et al. 1999, *A&A*, 349, L69S
 Simon, R., Jackson, J.M., Rathborne, J.M., & Chambers, E.T. 2006, *ApJ*, 639, 227
 Simon, R., Rathborne, J. M., Shah, R. Y., Jackson, J. M., Chambers, E. T. 2006, *ApJ*, 653, 1325
 Sofue, Y. 2006, *PASJ*, 58, 335
 Stolovy, S., Ramirez, S., Arendt, R. G., Cotera, A., Yusef-Zadeh, F. et al. 2006, *J. Phys. Conf. Ser*, 54, 176
 Taylor, G. B., Morris, M. & Schulman, E. 1993, *AJ*, 106, 1978
 Tsuboi, M., Handa, T., & Ukita, N. 1999, *ApJS*, 120, 1
 Wang Y., Zhang Q., Rathborne J.M., Jackson J., & Wu Y. 2006, *ApJL*, 651, L125
 Yusef-Zadeh, F., Hewitt, J. W., Arendt, R. G., Whitney, B., Rieke, G., et al. 2009, *ApJ*, 702, 178